The Association Between Coronary ^{18}F-Sodium Fluoride Uptake With Pro-Atherosclerosis Factors in Patients With Multivessel Coronary Artery Disease: A Mono-Centric Pilot Study

Wanwan Wen
Beijing An Zhen Hospital: Capital Medical University Affiliated Anzhen Hospital
Mingxin Gao
Beijing An Zhen Hospital: Capital Medical University Affiliated Anzhen Hospital
Mingkai Yun
Beijing An Zhen Hospital: Capital Medical University Affiliated Anzhen Hospital
Jingjing Meng
Beijing An Zhen Hospital: Capital Medical University Affiliated Anzhen Hospital
Ziwei Zhu
Beijing An Zhen Hospital: Capital Medical University Affiliated Anzhen Hospital
Wenyuan Yu
Beijing An Zhen Hospital: Capital Medical University Affiliated Anzhen Hospital
Marcus Hacker
Vienna General Hospital, Medical University of Viennasity Vienna
Yang Yu
Beijing An Zhen Hospital: Capital Medical University Affiliated Anzhen Hospital
Xiang Li
Vienna General Hospital, Medical University of Vienna
Xiaoli Zhang (xlzhang68@126.com)
Beijing An Zhen Hospital: Capital Medical University Affiliated Anzhen Hospital https://orcid.org/0000-0002-0770-5594

Research Article

Keywords: 18F-Sodium fluoride PET, peri-coronary adipose tissue, multivessel coronary artery disease, osteogenesis, inflammation

Posted Date: June 3rd, 2021

DOI: https://doi.org/10.21203/rs.3.rs-568886/v1

Abstract

Purpose: ^{18}F-Sodium fluoride (^{18}F-NaF) positron emission tomography (PET) is a novel approach to detect and quantify microcalcification in atherosclerosis. Peri-coronary adipose tissue (PCAT) is associated with vascular inflammation and high-risk atherosclerotic plaque. We aimed to assess the association between coronary ^{18}F-NaF uptake with pro-atherosclerosis factors in patients with multivessel coronary artery disease (CAD) and to explore the systematic vascular osteogenesis in the coronary artery and aorta in these patients.

Methods: Patients with multivessel CAD prospectively underwent cardiac computed tomography (CT) and ^{18}F-NaF PET/CT. PCAT density was measured in the coronary artery and the average PCAT value was calculated from the three coronary arteries in each patient. ^{18}F-NaF tissue-to-blood ratios (TBR) in the coronary artery ($TBR_{Coronary}$) and aorta (TBR_{Aorta}) were calculated. Correlations between coronary ^{18}F-NaF uptake with PCAT density, coronary artery calcium (CAC) burden, CAD risk factors, serum biomarkers, and aortic ^{18}F-NaF uptake were evaluated, respectively. Patients were categorized by a median of $TBR_{Coronary}$ 2.49.

Results: 100 multivessel CAD patients (64.00 [57.00 - 67.75] years; 76 men) were prospectively recruited. 6010 active aortic segments (TBR $\geq$ 1.6) were identified. $TBR_{Coronary}$ was significantly associated with the PCAT density ($r = 0.56$, $p < 0.001$) and CAC score ($r = 0.45$, $p < 0.001$). $TBR_{Coronary}$ was also significantly associated with the TBR_{Aorta} ($r = 0.42$, $p < 0.001$). In addition, patients with higher $TBR_{Coronary}$ showed elevated PCAT density (-75.89[-79.07 - -70.06] vs -84.54[-90.21 - -79.46]; $p < 0.001$) and CAC score (1495.20[619.80 - 2225.40] vs 273.75[116.73 - 1198.18]; $p < 0.001$) in comparsion patients with lower $TBR_{Coronary}$. $TBR_{Coronary}$ was correlated with the age ($r = 0.24$, $p = 0.019$) and the serum troponin I levels ($r = 0.22$, $p = 0.039$). There were no significant correlations between $TBR_{Coronary}$ with other conventional CAD risk factors and other serum biomarkers.

Conclusion: Coronary ^{18}F-NaF uptake was correlated with the PCAT density. A significant correlation between ^{18}F-NaF uptake in the coronary artery and aorta might indicate a systematic vascular osteogenesis in patients with multivessel CAD.

Introduction

Coronary atherosclerotic plaque rupture is the principal cause of acute coronary syndrome and a significant cause of sudden cardiac death and its prevention is a crucial adjective [1, 2]. During atherosclerosis progression, macrophage-derived cytokines induce osteogenic differentiation and mineralization of vascular cells, which suggests that pro-inflammatory molecules could promote atherosclerotic osteogenesis by regulating the differentiation of calcifying vascular cells [3]. Active microcalcifications in the atherosclerotic plaque is considered as a marker of cell death and inflammation and carries an increased risk of plaque rupture and associated complications [4]. ^{18}F-sodium fluoride

(^{18}F-NaF) has been used for bone positron emission tomography (PET) imaging to define osteogenic activity and its feasibility for identifying increased intraplaque osteogenic activity in vivo was appreciated [5, 6]. By providing molecular information vascular microcalcification, ^{18}F-NaF PET/computed tomography (CT) is potentially capable to identify high-risk atherosclerotic plaques in patients with multivessel coronary artery disease (CAD). Additionally, in complex cardiovascular diseases, the relevance of systemic causes of atherosclerosis development and progression is widely recognized, ^{18}F-NaF PET coud be a novel approach to visualize and quantify biochemical activity in systematic vasculature with high sensitivity.

Peri-coronary adipose tissue (PCAT) is a part of epicardial adipose tissue depot with brown and beige features, which is a source of some inflammatory mediators and pro-atherogenic mediators [7, 8]. Its closely near to the coronary artery tree has been implied to be potentially relevant for the development and progression of atherosclerosis by local inflammation and paracrine mechanisms [9, 10]. Increased density of PCAT plays an important role in the development of vascular inflammation and coronary atherosclerosis through bidirectional communication with the vessel wall at a cellular level [11, 12]. A recent large cohort study demonstrated that high PCAT density predicted all-cause and cardiac mortality and could enhance cardiac risk prediction and risk stratification by providing a quantitative measurement of coronary inflammation [13]. In addition, new-onset or rapid coronary calcification progression is associated with an enhanced risk for future CAD events and cardiovascular risk prediction can be improved by examining the coronary artery calcium (CAC) burden.

In the present study, we aimed to analyze the association between coronary artery osteogenic activity and conventional pro-atherosclerosis factors, including PCAT density, CAC burden, CAD risk factors, and serum biomarkers in patients with multivessel CAD. In addition, we also evaluated the systematic vascular osteogenesis in the coronary artery and aorta in these patients.

Material And Methods

Patient population

This observational cross-sectional study was a mono-centric pilot study to a prospective trial registered with the Chinese Clinical Trial Registry (ChiCTR1900022527). A total of 457 consecutive patients with CAD were prospectively recruited in Beijing Anzhen Hospital between February 2018 and April 2021. Inclusion in this study required angiographically confirmed multivessel CAD, defined as having at least 2 of 3 epicardial vessels with a stenosis ≥70% or left the main stenosis ≥50%. Patients were excluded if: 1) a recent myocardial infarction (< 4 weeks), 2) history of malignancy, acute or chronic inflammatory and autoimmune disease, 3) history of cardiovascular surgery or cardiac transplantation. Finally, a total of 100 multivessel CAD patients were recruited in our current study. The study flow chart is shown in Figure 1. The project was approved by the Medicine Ethics Committee of Beijing Anzhen Hospital (2018055X) and adhered to the principles laid out in the Declaration of Helsinki. Baseline characteristics of study population are listed in Table 1.

Analysis of CAC burden and PCAT on CT

All cardias CT scans were conducted using electrocardiography-gated cardiac CT using a 128-slice multi-detector computed tomography scanner (Biograph mCT, Siemens Healthcare, Erlangen, Germany). The scan parameters were: 128 x 0.6 mm collimation; tube voltage, 120 kV; gantry rotation time, 330ms; and tube current, 770-850 mAs. Coronary calcium was quantified on both a per-patient and per-segment level by an experienced observer (WW) using volume analysis software (Cascoring Siemens Healthcare, mCT). The CAC score was derived using the Agatston method [14]. To quantify the PCAT density, a CT attenuation threshold of -190 to -30 Hounsfield Units was used to isolate adipose tissue by Mimics Medical software (version 21.0; Materialise, Leuven, Belgium) [15], and the PCAT density was defined as the mean attenuation within such contamination-free volumes of interest and was measured in the reference region of the proximal left anterior descending (LAD), proximal left circumflex (LCX), and mid-right coronary artery (RCA) on axial CT images. For each coronary artery, five of regions of interest (ROIs, each ROI area = 3 mm^2) were manually placed on the region of distance the outer coronary artery wall equal in width to the vessel diameter [16]. The PCAT density of the LAD ($PCAT_{LAD}$), LCX ($PCAT_{LCX}$) and RCA ($PCAT_{RCA}$) was calculated by the average PCAT value from the value of five ROIs in LAD, LCX, and RCA, respectively. The PCAT density in each patient was calculated as the average PCAT value from three main coronary arteries (LAD, LCX, and RCA). PCAT density measurement by cardiac CT was performed by two experienced nuclear cardiologists (MJ and WW), who were blinded to the quantitative analysis data as well as ^{18}F-NaF PET/CT image analysis.

Cardiac ^{18}F-NaF PET/CT and image analysis

All patients were administered a target dose of ^{18}F-NaF (3.7 MBq/kg) intravenously and subsequently rested in a quiet environment for a 120-min uptake period, an electrocardiogram-gated cardiac ^{18}F-NaF PET/CT imaging (Biograph mCT, Siemens Medical Systems, Erlangen, Germany) was performed. A low-dose attenuation correction CT scan (120 kV, 50 mAs) was then acquired. The PET data were reconstructed using a point spread function + time of flight algorithm (time of flight + TrueX, Siemens Ultra-HD), with 5 iterations and 21 subsets. Due to the small size of the vulnerable plaques, an in-plane pixel size of 2 mm with a corresponding reconstructed image matrix size of 400×400 was used to achieve a high spatial resolution.

To evaluate the coronary ^{18}F-NaF uptake, the maximum standardized uptake value (SUV_{max}) (a validated measure of tissue radiotracer uptake) of LAD, LCX and RCA were quantified from ROIs by delimiting three-dimensional regions, respectively. The tissue-to-background ratios (TBR) in the LAD (TBR_{LAD}), LCX (TBR_{LCX}), and RCA (TBR_{RCA}) were then calculated by correction for background blood pool activity using the right atrium (mean SUV using cylindrical volumes-of-interest [radius: 10 mm; thickness: 5 mm] at the level of the RCA ostium). The TBR in the coronary artery ($TBR_{Coronary}$) was calculated as the average TBR value from three main coronary arteries (LAD, LCX, and RCA) in each patient.

The aortic (ascending aorta, aortic arch, descending aorta) ^{18}F-NaF uptake was determined by manually placing oval ROIs on the equatorial plane of these major arteries to avoid artifacts from the accumulation of ^{18}F-NaF in the vertebral body [17]. The SUV_{max} of ^{18}F-NaF avid focus more than 1.6 times the mean SUV of the right atrium blood pool was considered an abnormal aorta lesion. The number of lesions and SUV_{max} of each lesion in the aorta were recorded and measured. The TBR in the aorta (TBR_{Aorta}) was calculated by the average of lesions SUV_{max} in the aorta corrected by the mean of SUV in the right atrium.

Statistical analysis

All statistical analyses were performed using SPSS software (version 25, SPSS, Inc., Chicago, IL). Continuous variables were tested for normality using Shapiro-Wilk test and were presented as mean ± standard deviation or median (interquartile range) dependent on the distribution. Patients were divided dichotomously by the median $TBR_{Coronary}$ value into group 1 ($TBR_{Coronary} \geq 2.49$, n = 50) and group 2 ($TBR_{Coronary} < 2.49$, n = 50). Data were compared by using two-sample t-test or Mann-Whitney U tests. Categorical variables were summarized using frequencies and percentages and were compared by using a chi-squared test (with a Yates correction or a Fisher exact test for smaller sample sizes). Spearman's correlation analyses and multiple linear regression analyses were used to assess the correlations between the coronary ^{18}F-NaF uptake with the PCAT density, CAC burden, CAD risk factors, serum biomarkers, and aortic ^{18}F-NaF uptake, respectively. Bland-Altman analyses were employed to assess the repeatability of the PCAT density and coronary ^{18}F-NaF uptake (Additional file: Figure S1 and Figure S2). A 2-sided p-value < 0.05 was regarded as significant.

Results

Baseline clinical characteristics of the study population

A total of 100 multivessel CAD patients were enrolled (age 64.00 [57.00 - 67.75] years; 76 men; NYHA class III/IV: 63%; hyperlipidemia: 58%; hypertension: 71%), widespread utilization of secondary preventative therapies aspirin: 82%; stains: 87%; Beta-blocker: 75% (Table 1). The PCAT density and CAC score were -79.50 (-86.62 - -73.58) and 808.00 (213.30 - 1646.30), respectively. Serum biomarkers were presented in the following: high-density lipoprotein: 0.97 (0.85 - 1.13) mmol/L; low-density lipoprotein: 2.17 (1.81 - 2.86) mmol/L; high-sensitivity C-reactive protein: 2.56 (0.86 - 15.15) mg/L; interleukin-6: 6.40 (4.20 - 8.40) pg/mL; tumor necrosis factor alpha: 9.27 (7.50 - 13.30) pg/mL; creatinine clearance rate: 87.00 (70.00 - 101.00) mL/min; and troponin I: 0.01 (0.00-0.05) ng/mL.

Correlation between coronary ^{18}F-NaF uptake with PCAT density and calcium burden

As shown in Table 2, the $TBR_{Coronary}$ was significantly correlated with the PCAT density (r = 0.56, p < 0.001). There were weak correlations between the TBR value and the corresponding PCAT density in LAD, LCX, and RCA territories (r = 0.47, p < 0.001; r = 0.36, p < 0.001; r = 0.41, p < 0.001; respectively) (Figure 2). Per patient, we found that PCAT density was independently associated with the $TBR_{Coronary}$ (Beta = 0.489;

95% confidence interval [CI]: 0.032 - 0.067; p < 0.001) by multiple linear regression analyses (Demographics as covariates) (Table 3). In addition, the PCAT density was elevated in patients in group 1 in comparison with in group 2 (p < 0.001) (Supplemental file: Table S1).

There was a significant association between the $TBR_{Coronary}$ and the CAC score (r = 0.45, p < 0.001) (Table 2). The CAC score was significantly higher in group 1 compared with that in group 2 (p < 0.001) (Supplemental file: Table S1).

Correlation between coronary ^{18}F-NaF uptake and aortic ^{18}F-NaF uptake

On image analysis of aortic PET, we identified 6010 active segments in aorta. The $TBR_{Coronary}$ was significantly correlated with the TBR_{Aorta} in all individuals (r = 0.42, p < 0.001) (Table 2). Representative patients presenting in groups 1 and 2 are illustrated in Figures 3 and 4, respectively. Moreover, after adjustment confounding factors (age, gender, body mass index), we observed that the TBR_{Aorta} (Beta = 0.409; 95% CI: 0.215 - 0.619; p < 0.001) were independently associated with the $TBR_{Coronary}$ by multiple linear regression analyses (Table 3). The TBR_{Aorta} in group 1 was significantly higher than that in group 2 (p = 0.001) (Supplemental file: Table S1).

Correlation between CAD risk factors, serum biomarkers with coronary ^{18}F-NaF uptake and aortic ^{18}F-NaF uptake

Age in all individuals was significantly correlated with $TBR_{Coronary}$ (r = 0.24, p = 0.019) (Table 2) and TBR_{Aorta} (r = 0.29, p = 0.005) (Table 4). Patients in group 1 were relatively older (p = 0.002) (Supplemental file: Table S1).

Serum troponin I level in all individuals was correlated with $TBR_{Coronary}$ (r = 0.22, p = 0.039) (Table 2). There was no significant correlation between traditional CAD risk factors (eg. diabetes, hyperlipidemia, hypertension, smoker, family history of CAD, high-density lipoprotein, low-density lipoprotein, high-sensitivity C-reactive protein, interleukin-6, tumor necrosis factor alpha, and creatinine clearance rate) with neither $TBR_{Coronary}$ (Table 2) and TBR_{Aorta} (Table 4).

Discussion

In this present study, we investigated the correlations between coronary artery and aorta osteogenic activity with pro-atherosclerotic factors, including PCAT density, CAC score, and CAD risk factors in patients with multivessel CAD. We found that coronary ^{18}F-NaF uptake was significantly correlated with the PCAT density as well as the CAC score. Furthermore, a systematic osteogenesis activation in coronary artery and aorta was appreciated.

Atherosclerosis is a fundamental pathogenic process in many diseases, including cerebrovascular and cardiovascular diseases, aortic aneurysm/dissection, and arteriosclerosis obliterans. Plaque is known to

be the major characteristics of atherosclerosis and various pathophysiologic processes are involved in the formation and progression of atherosclerotic plaque, including inflammation, apoptosis, and mineralization [18, 19]. Inflammation mainly mediated by macrophages is involved at the beginning of the formation of plaque. Macrophages promote the proinflammatory milieu and send specific signals to vascular wall cells to initiate osteogenic differentiation. Once equilibrium in the arterial wall shifts toward calcification, deposition of hydroxyapatite could progress quickly, and gives rise to microcalcification, which is coalesce and ultimately pervade into the atherosclerotic plaque [20]. Microcalcification, which represents a specific phase in the evolution of an atheroma, is a key feature of atherosclerotic plaque rupture, that is embedded in the fibrous cap of atherosclerotic plaques and, then lead to considerable stress accumulation in the fibrous cap and destabilize the structural integrity of the fibrous cap [21]. ^{18}F-NaF is a radiotracer that preferentially identifies microcalcification in arteries by binding to hydroxyapatite. Therefore, vascular ^{18}F-NaF PET may identify high-risk atherosclerotic plaque lesions and enable the quantification of osteogenic activity before therapeutic interventions, thereby providing a powerful tool for improving patient risk stratification.

PCAT is an ectopic thoracic fat tissue located between the visceral layer of the pericardium and the myocardium, surrounding the coronary artery tree [7, 8, 10]. A large body of evidence, including experimental and clinical studies, has demonstrated that PCAT is a recognized source of pro-inflammatory mediators in high-risk cardiac patients, which can directly modulate the coronary artery through the mechanism of paracrine and autocrine [9, 22]. PCAT exhibits a broadly pathogenic mRNA profile, and it is associated with the presence and incidence of cardiovascular and cerebrovascular events independent of traditional risk factors [23]. Moreover, several studies have indicated that the relationship of adipose tissue and the vascular wall is a complex interaction, PCAT releases a wide range of bioactive molecules that exert endocrine and paracrine effects on the vascular lipid metabolism and vascular inflammation [10, 24]. ^{18}F-NaF PET/CT has emerged as a noninvasive quantitative imaging modality and is able to measure the microcalcification activity in the vasculature [4, 25]. In this study, we found a significant correlation between coronary ^{18}F-NaF activity and PCAT density, which was concordant with findings by Kwecinski et al [26, 27], who demonstrated an association of increased PCAT CT attenuation with higher ^{18}F-NaF PET activity in patients with high-risk plaques. In contrast to previous studies, we conducted an observational cross-sectional study including 100 multivessel CAD patients and performed a delay PET scans (120-min) with potentially improved imaging contrast. We observed that PCAT density was significantly increased in patients with higher coronary ^{18}F-NaF uptake, and it was independently associated with the coronary ^{18}F-NaF uptake after adjustment for confounding factors.

Pioneering studies demonstrated that the coronary ^{18}F-NaF uptake was significantly correlated with the CAC score and the progression of coronary calcification [17, 28]. Increased coronary ^{18}F-NaF uptake was associated with more rapid progression of coronary calcification at one year in patients with clinically stable multivessel CAD [28]. And intriguingly, we also found that coronary ^{18}F-NaF uptake was correlated with the calcium burden in the coronary artery assessed by cardiac CT. These results may indicate that the underlying correlation between the accumulation of ^{18}F-NaF and the incremental change in calcified

plaque progression. Moreover, McKenney-Drake et al demonstrated that ^{18}F-NaF uptake in all vascular segments was significantly correlated with age in patients with chest pain syndromes [29]. In our observation, increased coronary and aortic ^{18}F-NaF uptake were also presented in older patients, which might raise a intriguing possibility that intense hydroxyapatite deposition was developed in older patients.

Cardiac troponin I was used to detect myocardial necrosis as the preferred biomarker in the diagnostic of myocardial infarction [30]. Joshi et al reported an association between increased coronary ^{18}F-NaF uptake and higher plasma high-sensitivity cardiac troponin I concentrations in patients with stable CAD [31]. In this study, we also observed that serum troponin I level was associated with coronary ^{18}F-NaF uptake in multivessel CAD patients. In fact, silent plaque rupture and subclinical plaque thrombus formation are frequent incidental post-mortem findings in patients with multivessel CAD. These results suggests that coronary ^{18}F-NaF uptake may identify high risk plaques which might be associated with thrombus formation and subclinical myocardial injury from microemboli.

The prevalence and development of aortic plaque are closely related to coronary artery atherosclerosis, consistent with an underlying systemic vascular atherosclerotic process. McGill et al found a concordant pattern of raised fatty streaks in the abdominal aorta and the right coronary artery [32]. In addition, a recent cross-sectional observation study demonstrated that asymptomatic and spontaneous aortic plaque rupture was detected in 80% of patients suspected or diagnosed with CAD [33]. The present study revealed an interactive connection of systemic osteogenesis within large artery. It might demonstrate a concomitant microcalcification activation in symptomatic CAD patients. Thus, simultaneous screening the osteogenesis in the multiple vasculatures may clarify the precise pathophysiological conditions and mechanisms underlying multivascular disease.

Study Limitations

This study had several limitations. First, this was a single-center study given limited number of observations, and bias in patient selection was possible; however, adjustments were made for the confounding effects of risk factors for the association of PCAT density and coronary ^{18}F-NaF activity. Second, partial volume effects and cardiac motion could have affected the PET quantification in coronary artery lesions. Third, CT angiography is not performed in this study cohort. Finally, the patient outcome assessment is lacking from the current study.

Conclusion

In multivessel CAD patients, increased coronary ^{18}F-NaF uptake was significantly associated with the classic pro-atherosclerosis factors, including PCAT density and CAC score. We also observed an ^{18}F-NaF uptake cross-talk between the coronary artery and aorta. Patients' clinical research to validate that such a pro-atherosclerosis axis translates into a better outcome is warranted.

Declarations

Funding information:

We thank the Key Medical Specialty Program of Sailing Plans organized by Beijing Municipal Administration of Hospitals (grant numbers: ZYLX202110), the National Natural Science Foundation of China (grant numbers: 81871377, 81571717), and the Research on Clinical Characteristics of Capital (grant number: Z181100001718071) for supporting this research.

Conflict of interest:

None

Availability of data and material:

The datasets used and analyzed during the current study are available from the corresponding author on reasonable request.

Authors' contributions:

Xiang Li and Xiaoli Zhang have substantial contributions to the supervision of the study, Wanwan Wen, Mingxin Gao, Mingkai Yun, Jingjing Meng, Ziwei Zhu, and Wenyuan Yu have substantial contributions to the acquisition, analysis, and interpretation of data for the research. Wanwan Wen and Mingxin Gao have substantial contributions to draft this paper. Marcus Hacker, Yang Yu, Xiang Li and Xiaoli Zhang have substantial contributions to revise this paper.

Ethical approval and Consent to paticipate:

This study was registered with the Chinese Clinical Trial Registry (No. ChiCTR1900022527) was approved by the Medicine Ethics Committee of Beijing Anzhen Hospital (2018055X).

Consent for publication:

Not applicable

Acknowledgements:

We are extremely grateful to Dr. Wei Yu, Department of Radiology, Beijing Anzhen Hospital, Capital Medical University Beijing, for her advice on improving the manuscript.

References

1. Libby P, Pasterkamp G, Crea F, Jang IK. Reassessing the Mechanisms of Acute Coronary Syndromes. Circ Res. 2019;124:150–60. doi:10.1161/circresaha.118.311098.

2. Ferraro RA, van Rosendael AR, Lu Y, Andreini D, Al-Mallah MH, Cademartiri F, et al. Non-obstructive high-risk plaques increase the risk of future culprit lesions comparable to obstructive plaques without high-risk features: the ICONIC study. Eur Heart J Cardiovasc Imaging. 2020;21:973–80. doi:10.1093/ehjci/jeaa048.
3. Radcliff K, Tang TB, Lim J, Zhang Z, Abedin M, Demer LL, et al. Insulin-like growth factor-I regulates proliferation and osteoblastic differentiation of calcifying vascular cells via extracellular signal-regulated protein kinase and phosphatidylinositol 3-kinase pathways. Circ Res. 2005;96:398–400. doi:10.1161/01.RES.0000157671.47477.71.
4. Irkle A, Vesey AT, Lewis DY, Skepper JN, Bird JL, Dweck MR, et al. Identifying active vascular microcalcification by ^{18}F-sodium fluoride positron emission tomography. Nat Commun. 2015;6:7495. doi:10.1038/ncomms8495.
5. Høilund-Carlsen PF, Sturek M, Alavi A, Gerke O. Atherosclerosis imaging with ^{18}F-sodium fluoride PET: state-of-the-art review. Eur J Nucl Med Mol Imaging. 2020;47:1538–51. doi:10.1007/s00259-019-04603-1.
6. Li L, Li X, Jia Y, Fan J, Wang H, Fan C, et al. Sodium-fluoride PET-CT for the non-invasive evaluation of coronary plaques in symptomatic patients with coronary artery disease: a cross-correlation study with intravascular ultrasound. Eur J Nucl Med Mol Imaging. 2018;45:2181–9. doi:10.1007/s00259-018-4122-0.
7. Sacks HS, Fain JN. Human epicardial adipose tissue: a review. Am Heart J. 2007;153:907–17. doi:10.1016/j.ahj.2007.03.019.
8. Buschmann K, Wrobel J, Chaban R, Rosch R, Ghazy A, Hanf A, et al. Body Mass Index (BMI) and Its Influence on the Cardiovascular and Operative Risk Profile in Coronary Artery Bypass Grafting Patients: Impact of Inflammation and Leptin. Oxid Med Cell Longev. 2020;2020:5724024. doi:10.1155/2020/5724024.
9. Margaritis M, Antonopoulos AS, Digby J, Lee R, Reilly S, Coutinho P, et al. Interactions between vascular wall and perivascular adipose tissue reveal novel roles for adiponectin in the regulation of endothelial nitric oxide synthase function in human vessels. Circulation. 2013;127:2209–21. doi:10.1161/CIRCULATIONAHA.112.001133.
10. Mancio J, Barros AS, Conceicao G, Pessoa-Amorim G, Santa C, Bartosch C, et al. Epicardial adipose tissue volume and annexin A2/fetuin-A signalling are linked to coronary calcification in advanced coronary artery disease: Computed tomography and proteomic biomarkers from the EPICHEART study. Atherosclerosis. 2020;292:75–83. doi:10.1016/j.atherosclerosis.2019.11.015.
11. Bettencourt N, Toschke AM, Leite D, Rocha J, Carvalho M, Sampaio F, et al. Epicardial adipose tissue is an independent predictor of coronary atherosclerotic burden. Int J Cardiol. 2012;158:26–32. doi:10.1016/j.ijcard.2010.12.085.
12. Yamashita K, Yamamoto MH, Igawa W, Ono M, Kido T, Ebara S, et al. Association of Epicardial Adipose Tissue Volume and Total Coronary Plaque Burden in Patients with Coronary Artery Disease. Int Heart J. 2018;59:1219–26. doi:10.1536/ihj.17-709.

13. Oikonomou EK, Marwan M, Desai MY, Mancio J, Alashi A, Hutt Centeno E, et al. Non-invasive detection of coronary inflammation using computed tomography and prediction of residual cardiovascular risk (the CRISP CT study): a post-hoc analysis of prospective outcome data. Lancet. 2018;392:929–39. doi:10.1016/S0140-6736(18)31114-0.
14. Agatston AS, Janowitz WR, Hildner FJ, Zusmer NR, Viamonte M Jr, Detrano R. Quantification of coronary artery calcium using ultrafast computed tomography. J Am Coll Cardiol. 1990;15:827–32. doi:10.1016/0735-1097(90)90282-t.
15. Scheidt M, Wesolowski M, Salazar D, Garbis N. A 3-dimensional comparison of hand and power reamers in accuracy of glenoid retroversion correction. J Shoulder Elbow Surg. 2020;29:609–16. doi:10.1016/j.jse.2019.08.011.
16. Antonopoulos AS, Sanna F, Sabharwal N, Thomas S, Oikonomou EK, Herdman L, et al. Detecting human coronary inflammation by imaging perivascular fat. Sci Transl Med. 2017;9. doi:10.1126/scitranslmed.aal2658.
17. Ishiwata Y, Kaneta T, Nawata S, Hino-Shishikura A, Yoshida K, Inoue T. Quantification of temporal changes in calcium score in active atherosclerotic plaque in major vessels by ^{18}F-sodium fluoride PET/CT. Eur J Nucl Med Mol Imaging. 2017;44:1529–37. doi:10.1007/s00259-017-3680-x.
18. Otsuka F, Sakakura K, Yahagi K, Joner M, Virmani R. Has our understanding of calcification in human coronary atherosclerosis progressed? Arterioscler Thromb Vasc Biol. 2014;34:724–36. doi:10.1161/atvbaha.113.302642.
19. Nakahara T, Strauss HW. From inflammation to calcification in atherosclerosis. Eur J Nucl Med Mol Imaging. 2017;44:858–60. doi:10.1007/s00259-016-3608-x.
20. Aikawa E, Nahrendorf M, Figueiredo JL, Swirski FK, Shtatland T, Kohler RH, et al. Osteogenesis associates with inflammation in early-stage atherosclerosis evaluated by molecular imaging in vivo. Circulation. 2007;116:2841–50. doi:10.1161/circulationaha.107.732867.
21. Hutcheson JD, Maldonado N, Aikawa E. Small entities with large impact: microcalcifications and atherosclerotic plaque vulnerability. Curr Opin Lipidol. 2014;25:327–32. doi:10.1097/mol.0000000000000105.
22. Mazurek T, Zhang L, Zalewski A, Mannion JD, Diehl JT, Arafat H, et al. Human epicardial adipose tissue is a source of inflammatory mediators. Circulation. 2003;108:2460–6. doi:10.1161/01.Cir.0000099542.57313.C5.
23. Toya T, Corban MT, Imamura K, Bois JP, Gulati R, Oh JK, et al. Coronary perivascular epicardial adipose tissue and major adverse cardiovascular events after ST segment-elevation myocardial infarction. Atherosclerosis. 2020;302:27–35. doi:10.1016/j.atherosclerosis.2020.04.012.
24. Ng AC, Goo SY, Roche N, van der Geest RJ, Wang WY. Epicardial Adipose Tissue Volume and Left Ventricular Myocardial Function Using 3-Dimensional Speckle Tracking Echocardiography. Can J Cardiol. 2016;32:1485–92. doi:10.1016/j.cjca.2016.06.009.
25. Tzolos E, Dweck MR. ^{18}F-NaF for Imaging Microcalcification Activity in the Cardiovascular System. Arterioscler Thromb Vasc Biol. 2020:Atvbaha120313785. doi:10.1161/atvbaha.120.313785.

26. Kwiecinski J, Dey D, Cadet S, Lee SE, Otaki Y, Huynh PT, et al. Peri-Coronary Adipose Tissue Density Is Associated With ^{18}F-Sodium Fluoride Coronary Uptake in Stable Patients With High-Risk Plaques. JACC Cardiovasc Imaging. 2019;12:2000–10. doi:10.1016/j.jcmg.2018.11.032.
27. Kitagawa T, Nakamoto Y, Fujii Y, Sasaki K, Tatsugami F, Awai K, et al. Relationship between coronary arterial ^{18}F-sodium fluoride uptake and epicardial adipose tissue analyzed using computed tomography. Eur J Nucl Med Mol Imaging. 2020;47:1746–56. doi:10.1007/s00259-019-04675-z.
28. Doris MK, Meah MN, Moss AJ, Andrews JPM, Bing R, Gillen R, et al. Coronary ^{18}F-Fluoride Uptake and Progression of Coronary Artery Calcification. Circ Cardiovasc Imaging. 2020;13:e011438. doi:10.1161/circimaging.120.011438.
29. McKenney-Drake ML, Moghbel MC, Paydary K, Alloosh M, Houshmand S, Moe S, et al. ^{18}F-NaF and ^{18}F-FDG as molecular probes in the evaluation of atherosclerosis. Eur J Nucl Med Mol Imaging. 2018;45:2190–200. doi:10.1007/s00259-018-4078-0.
30. Roffi M, Patrono C, Collet JP, Mueller C, Valgimigli M, Andreotti F, et al. 2015 ESC Guidelines for the management of acute coronary syndromes in patients presenting without persistent ST-segment elevation: Task Force for the Management of Acute Coronary Syndromes in Patients Presenting without Persistent ST-Segment Elevation of the European Society of Cardiology (ESC). Eur Heart J. 2016;37:267–315. doi:10.1093/eurheartj/ehv320.
31. Joshi NV, Vesey AT, Williams MC, Shah AS, Calvert PA, Craighead FH, et al. ^{18}F-fluoride positron emission tomography for identification of ruptured and high-risk coronary atherosclerotic plaques: a prospective clinical trial. Lancet. 2014;383:705–13. doi:10.1016/s0140-6736(13)61754-7.
32. McGill HC Jr, McMahan CA, Zieske AW, Sloop GD, Walcott JV, Troxclair DA, et al. Associations of coronary heart disease risk factors with the intermediate lesion of atherosclerosis in youth. The Pathobiological Determinants of Atherosclerosis in Youth (PDAY) Research Group. Arterioscler Thromb Vasc Biol. 2000;20:1998–2004. doi:10.1161/01.atv.20.8.1998.
33. Komatsu S, Yutani C, Ohara T, Takahashi S, Takewa M, Hirayama A, et al. Angioscopic Evaluation of Spontaneously Ruptured Aortic Plaques. J Am Coll Cardiol. 2018;71:2893–902. doi:10.1016/j.jacc.2018.03.539.

Abbreviations

^{18}F-NaF = ^{18}F-sodium fluoride

CAC = Coronary artery calcium

CAD = Coronary heart disease

CI = Confidence interval

CT = Computed tomography

LAD = Left anterior descending

LCX = Left circumflex

PCAT = Peri-coronary adipose tissue

PET = Positron emission tomography

RCA = Right coronary artery

ROIs = Regions of interest

SUV_{max} = Maximum standardized uptake value

TBR = Tissue-to-background ratios

Tables

Table 1 Baseline clinical characteristics of the study population

	n = 100
Baseline characteristics	
Age, years	64.00 (57.00 - 67.75)
Men, n (%)	76 (76.00)
BMI, kg/m^2	24.88 (23.08 - 27.33)
LVEF, %	59.00 (48.50 - 65.00)
Systolic blood pressure, mmHg	129.00 (120.00 - 141.75)
Diastolic blood pressure, mmHg	73.00 (67.00 - 79.00)
NYHA class III/IV, n (%)	63 (63.00)
Diabetes, n (%)	38 (38.00)
Hyperlipidemia, n (%)	58 (58.00)
Hypertension, n (%)	71 (71.00)
Smoker, n (%)	57 (57.00)
Family history of CAD, n (%)	35 (35.00)
Serum biomarkers	
High-density lipoprotein, mmol/L	0.97 (0.85 - 1.13)
Low-density lipoprotein, mmol/L	2.17 (1.81 - 2.86)
High-sensitivity C-reactive protein, mg/L	2.56 (0.86 - 15.15)
Interleukin-6, pg/mL	6.40 (4.20 - 8.40)
Tumor necrosis factor alpha, pg/mL	9.27 (7.50 - 13.30)
Creatinine clearance rate, mL/min	87.00 (70.00 - 101.00)
Troponin I, ng/mL	0.01 (0.00-0.05)
Medications, n (%)	
Aspirin	82 (82.00)
Statins	87 (87.00)
ACEIs/ARBs	32 (32.00)
Beta-blocker	75 (75.00)
CT	
Coronary artery calcium score	808.00 (213.30 - 1646.30)

PCAT	-79.50 (-86.62 - -73.58)
$PCAT_{LAD}$	-81.81 (-90.72 - -74.39)
$PCAT_{LCX}$	-78.20 (-86.85 - -70.60)
$PCAT_{RCA}$	-77.29 (-86.34 - -69.62)
PET/CT	
$TBR_{Coronary}$	2.48 (1.86 - 3.09)
TBR_{LAD}	2.86 (2.04 - 3.77)
TBR_{LCX}	2.20 (1.73 - 2.83)
TBR_{RCA}	2.20 (1.64 - 2.75)
TBR_{Aorta}	2.31 (1.96 - 3.23)

Data are presented as median (25th to 75th percentile) or n (%).

ACEI = angiotensin-converting enzyme inhibitor; ARB = angiotensin receptor blocker; BMI = body-mass index; CAD = coronary artery disease; CT = computed tomography; LVEF = left ventricular ejection function; NYHA = New York Heart Association; LAD = left anterior descending; LCX = left circumflex; PCAT = peri-coronary adipose tissue; PET/CT = positron emission tomography/computed tomography; RCA = right coronary artery; TBR = tissue-to-background ratio

Table 2 Correlation between the coronary TBR and clinical variables

	$TBR_{Coronary}$	
	r	P
Baseline characteristics		
Age, years	0.24	0.019
Men, n (%)	0.15	0.16
BMI, kg/m^2	0.03	0.79
LVEF, %	-0.13	0.24
Systolic blood pressure, mmHg	0.21	0.048
Diastolic blood pressure, mmHg	0.06	0.59
NYHA class III/IV, n (%)	0.06	0.58
Diabetes, n (%)	0.07	0.50
Hyperlipidemia, n (%)	0.07	0.52
Hypertension, n (%)	0.15	0.16
Smoker, n (%)	0.12	0.24
Family history of CAD, n (%)	0.07	0.51
Serum biomarkers		
High-density lipoprotein, mmol/L	0.06	0.56
Low-density lipoprotein, mmol/L	-0.05	0.61
High-sensitivity C-reactive protein, mg/L	0.04	0.72
Interleukin-6, pg/mL	0.19	0.11
Tumor necrosis factor alpha, pg/mL	-0.02	0.80
Creatinine clearance rate, mL/min	0.11	0.29
Troponin I, ng/mL	0.22	0.039
Medications, n (%)		
Aspirin	0.02	0.85
Statins	0.03	0.77
ACEIs/ARBs	0.11	0.31
Beta-blocker	0.02	0.85
CT		

Coronary artery calcium score	0.45	<0.001
PCAT	0.56	<0.001
PET/CT		
TBR_{Aorta}	0.42	<0.001

ACEI = angiotensin-converting enzyme inhibitor; ARB = angiotensin receptor blocker; BMI = body-mass index; CAD = coronary artery disease; CT = computed tomography; LVEF = left ventricular ejection function; NYHA = New York Heart Association; PCAT = peri-coronary adipose tissue; PET/CT = positron emission tomography/computed tomography; TBR = tissue-to-background ratio

Table 3 Univariate and multivariate linear regression analysis for coronary TBR

	Univariate		Model 1	
	Beta (95%CI)	P	Beta (95%CI)	P
PCAT	0.508 (0.033 - 0.069)	<0.001	0.489 (0.032 - 0.067)	<0.001
TBR_{Aorta}	0.446 (0.267 - 0.643)	<0.001	0.409 (0.215 - 0.619)	<0.001

Model1: adjusted for age, gender, BMI.

Table 4 Correlation between the aortic TBR and clinical variables

	TBR_{Aorta}	
	r	P
Baseline characteristics		
Age, years	0.29	0.005
Men, n (%)	0.15	0.16
BMI, kg/m^2	0.09	0.39
LVEF, %	-0.10	0.37
Systolic blood pressure, mmHg	0.11	0.32
Diastolic blood pressure, mmHg	-0.22	0.040
NYHA class III/IV, n (%)	-0.15	0.16
Diabetes, n (%)	0.12	0.26
Hyperlipidemia, n (%)	-0.09	0.39
Hypertension, n (%)	0.01	0.94
Smoker, n (%)	-0.01	0.91
Family history of CAD, n (%)	-0.23	0.026
Serum biomarkers		
High-density lipoprotein, mmol/L	-0.07	0.50
Low-density lipoprotein, mmol/L	-0.11	0.30
High-sensitivity C-reactive protein, mg/L	-0.11	0.28
Interleukin-6, pg/mL	0.10	0.38
Tumor necrosis factor alpha, pg/mL	-0.03	0.79
Creatinine clearance rate, mL/min	-0.10	0.35
Troponin I, ng/mL	-0.06	0.58
Medications, n (%)		
Aspirin	0.01	0.92
Statins	-0.12	0.28
ACEIs/ARBs	-0.09	0.39
Beta-blocker	0.15	0.18
CT		

Coronary artery calcium score	0.17	0.13
PCAT	0.13	0.23

r: Spearman correlation coefficients

ACEI = angiotensin-converting enzyme inhibitor; ARB = angiotensin receptor blocker; BMI = body-mass index; CAD = coronary artery disease; CT = computed tomography; LVEF = left ventricular ejection function; NYHA = New York Heart Association; PCAT = peri-coronary adipose tissue; PET/CT = positron emission tomography/computed tomography; TBR = tissue-to-background ratio.

BMI = body-mass index; CI = confidence interval; PCAT = peri-coronary adipose tissue; TBR = tissue-to-background ratio.

Figures

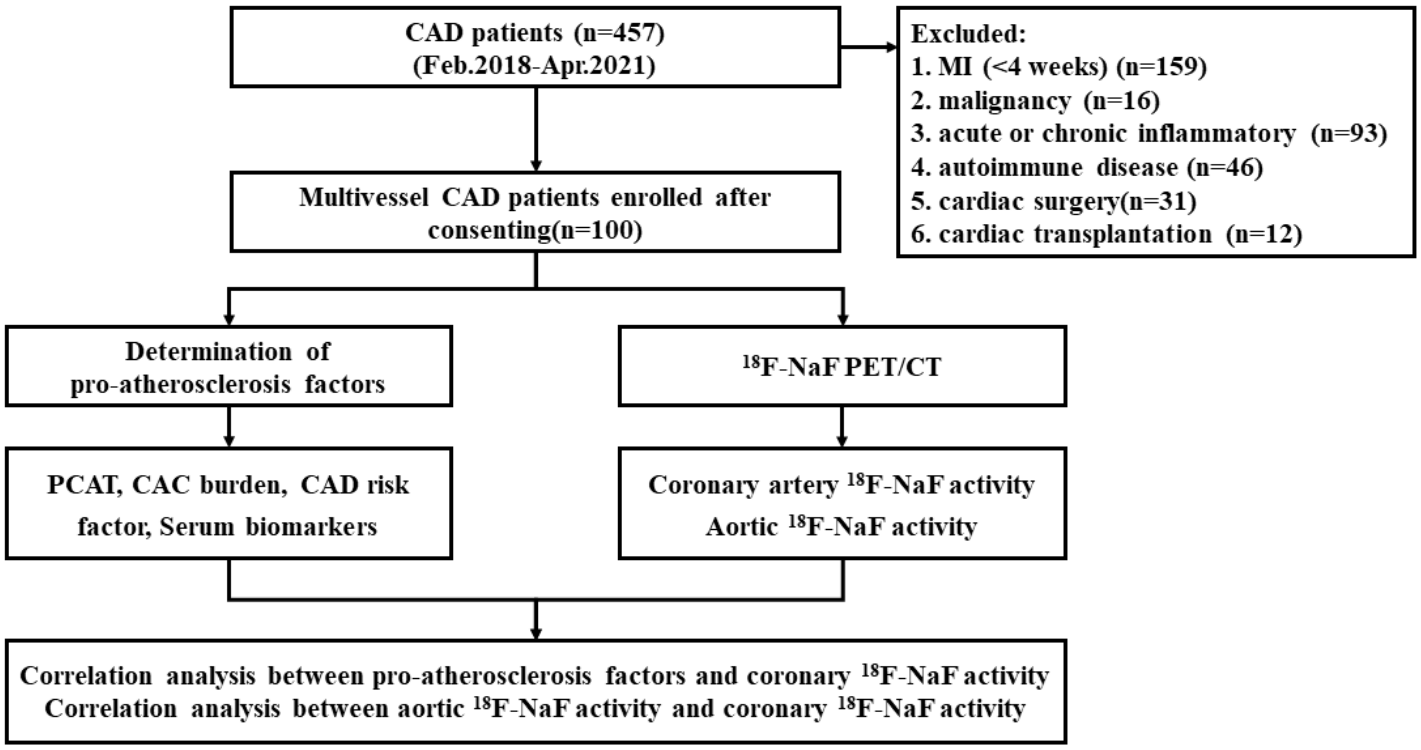

Figure 1

Study design flowchart. 18F-NaF = 18F-sodium fluoride; CAC = Coronary artery calcium score; CAD = coronary artery disease; MI = myocardial infarction; PCAT = peri-coronary adipose tissue; PET/CT = positron emission tomography/computed tomography.

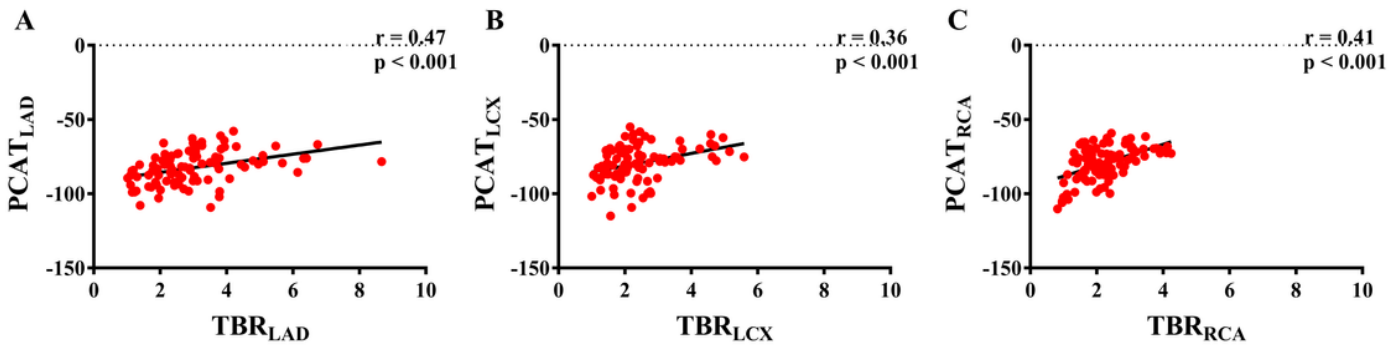

Figure 2

Scatterplots of PCATLAD vs TBRLAD (A), PCATLCX vs TBRLCX (B), PCATRCA vs TBRRCA (C). r = spearman correlation coefficients; LAD = left anterior descending; LCX = left circumflex; PCAT = peri-coronary adipose tissue; RCA = right coronary artery; TBR = tissue-to-background ratio

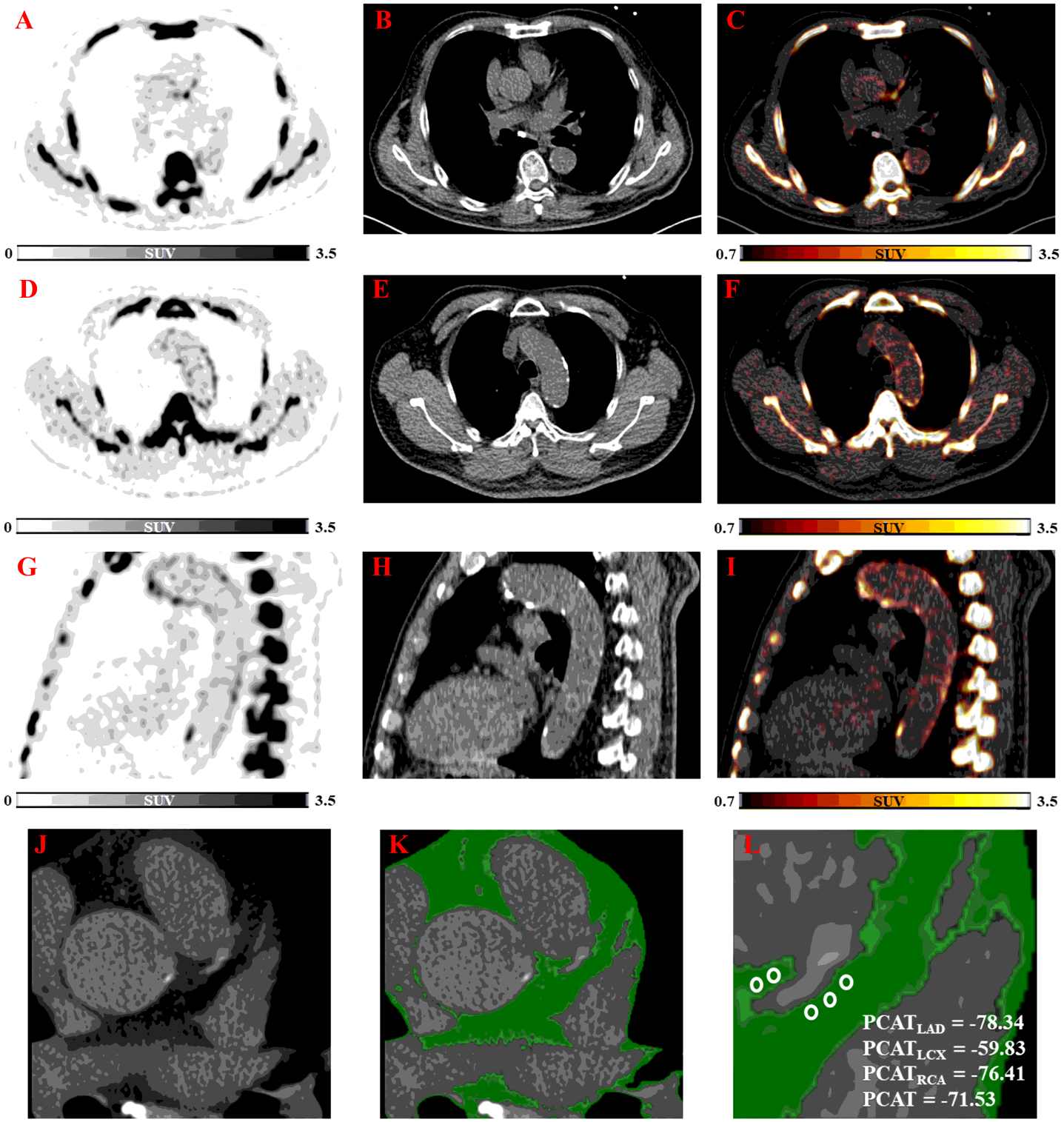

Figure 3

Representative case showing the relationship between coronary TBR with aortic TBR and PCAT in patients with prominent 18F-NaF uptake. Patient (male; 64y; TBRCoronary: 4.55; TBRAorta: 4.85; PCAT: -71.53; Coronary artery calcium score: 2995.50) suffered multivessel lesions presenting intense focal 18F-NaF uptake in left anterior descending artery overlying existing extensive coronary calcium (ABC), coupled with increased 18F-NaF uptake in aortic arch (DEF) and descending aorta (GHI), and with intense

PCAT density (JKL). Epicardial adipose area (green) for placing five regions of interest (3 mm2) and measuring PCAT density. 18F-NaF = 18F-sodium fluoride; PCAT = peri-coronary adipose tissue; TBR = tissue-to-background ratio

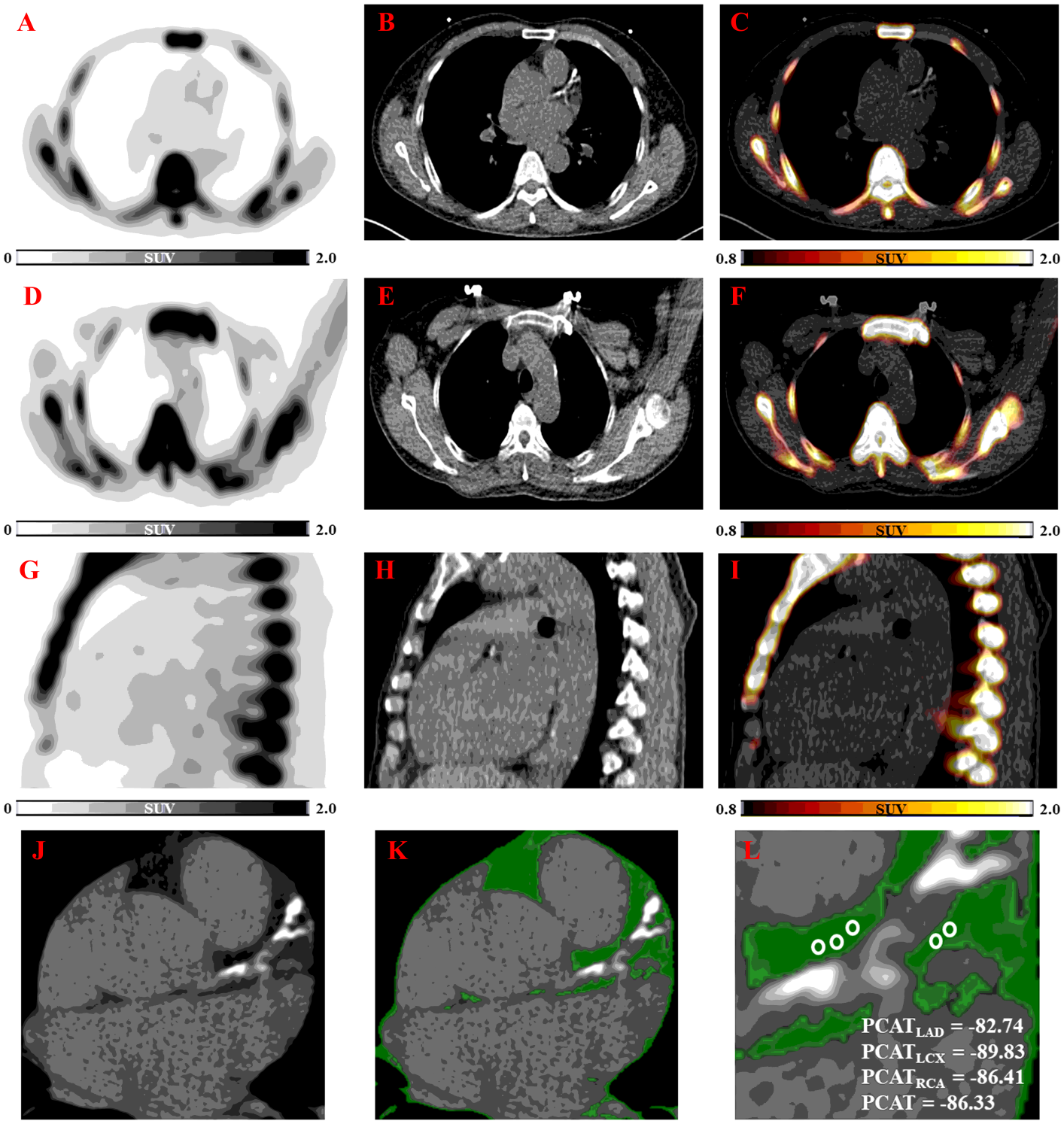

Figure 4

Representative case showing the relationship between coronary TBR and aortic TBR in patients with negative 18F-NaF uptake. Patient (male; 53y; TBRCoronary: 2.46; TBRAorta: 2.20; PCAT: -86.33; Coronary

artery calcium score: 792.90) who suffered multivessel lesions without 18F-NaF uptake in the left anterior descending artery but existing coronary calcium in this region (ABC), and without 18F-NaF uptake in the aortic arch (DEF) and descending aorta (GHI), and with lower PCAT density (JKL). Epicardial adipose area (green) for placing five regions of interest (3 mm2) and measuring PCAT density. 18F-NaF = 18F-sodium fluoride; PCAT = peri-coronary adipose tissue; TBR = tissue-to-background ratio

Supplementary Files

This is a list of supplementary files associated with this preprint. Click to download.

- SupplementaryMaterial.pdf